

# Vision without Images: End-to-End Computer Vision from Single Compressive Measurements

Fengpu Pan<sup>1</sup>, Heting Gao<sup>2</sup>, Jiangtao Wen<sup>3</sup>, Yuxing Han<sup>1</sup>,

<sup>1</sup>Tsinghua University

<sup>2</sup>Southern University of Science and Technology

<sup>3</sup>New York University

pfp23@mails.tsinghua.edu.cn, 12210816@mail.sustech.edu.cn, jw9263@nyu.edu, yuxinghan@sz.tsinghua.edu.cn

## Abstract

Snapshot Compressed Imaging (SCI) offers high-speed, low-bandwidth, and energy-efficient image acquisition, but remains challenged by low-light and low signal-to-noise ratio (SNR) conditions. Moreover, practical hardware constraints in high-resolution sensors limit the use of large frame-sized masks, necessitating smaller, hardware-friendly designs. In this work, we present a novel SCI-based computer vision framework using pseudo-random binary masks of only  $8 \times 8$  in size for physically feasible implementations. At its core is CompDAE, a Compressive Denoising Autoencoder built on the STFormer architecture, designed to perform downstream tasks—such as edge detection and depth estimation—directly from noisy compressive raw pixel measurements without image reconstruction. CompDAE incorporates a rate-constrained training strategy inspired by BackSlash to promote compact, compressible models. A shared encoder paired with lightweight task-specific decoders enables a unified multi-task platform. Extensive experiments across multiple datasets demonstrate that CompDAE achieves state-of-the-art performance with significantly lower complexity, especially under ultra-low-light conditions where traditional CMOS and SCI pipelines fail.

## Introduction

Traditional computer vision tasks including video classification (Karpathy et al. 2014), object detection and tracking (Wang and Yeung 2013; Girshick et al. 2014), and monocular depth estimation (Birkel, Wofk, and Müller 2023; Piccinelli et al. 2024; Bochkovskii et al. 2024) are typically performed in the RGB domain using spatial and temporal samples captured by CMOS active pixel sensors (APS). These systems rely heavily on high-throughput image signal processing (ISP) pipelines for denoising (Guo, Han, and Wen 2019; Li et al. 2021), demosaicing, and enhancement, resulting in high power consumption, significant latency, and bandwidth bottlenecks. The growing resolution of sensors exacerbates computational burdens in conventional vision pipelines, similar to “looking for needles in a haystack”. This motivates moving toward new imaging modalities such as compressive sensing (Candes and Tao 2005; Candès, Romberg, and Tao 2006; Baraniuk et al. 2008) based Snapshot Compressed Imaging (SCI (Hitomi et al. 2011; Reddy, Veeraraghavan, and Chellappa 2011; Llull et al. 2013; Gao et al. 2014; Yuan and Pang 2016)), where temporal encod-

ing via spatially varying masks allows multiple high-speed frames to be collapsed into a single 2D measurement, enabling dramatic reductions in bandwidth and energy consumption. SCI, however, still faces a fundamental hardware feasibility barrier to adoption. SCI systems typically require large, frame-sized spatial modulation masks to satisfy the Restricted Isometry Property (RIP). One approach to implementing masks is to load them from external memory and project the patterns onto the pixel array prior to each exposure (Gulve et al. 2022). However, when the masks are large, this method introduces substantial latency, power consumption, and system complexity. A more efficient alternative is to directly control pixel states via dedicated external signal lines (Gulve et al. 2022). Yet, as control lines are typically  $0.05\text{--}1\mu\text{m}$  wide and separated by similar spacing, due to physical constraints, each pixel can accommodate at most around 10 such lines. This imposes a stringent upper limit on mask size, making large dynamic masks infeasible for practical sensor integration.

Meanwhile, low-light and low signal-to-noise ratio (SNR) conditions are particularly challenging for vision systems based on both ASPs and SCI, yet critically important in scenarios such as autonomous driving and robotics. These conditions give rise to complex noise patterns, commonly modeled as Poisson-Gaussian noise (Foi et al. 2008). In dynamic scenes, where signal intensity fluctuates over time, the Poisson noise becomes non-stationary and temporally correlated (Ottewill and Rahman 1997; Sun et al. 2024), deviating from the conventional memoryless assumption. Existing denoising neural networks (Khademi et al. 2021) rarely account for such temporal dependencies, and robust computer vision under extreme low-light remains an open challenge (Dong et al. 2011).

To overcome these issues, we propose an end-to-end SCI-based vision system that operates directly on raw measurements using pseudo-random binary spatial modulation masks that are only  $8 \times 8$  in size, much smaller than conventionally needed for SCI and well-suited to existing CMOS implementations, enabling low-latency, low-power vision at the sensor level. Instead of reconstructing full video frames then applying computer vision algorithms using reconstructed full frames (Kwan et al. 2019), we design a unified model that performs vision tasks directly in the compressive measurement domain. While some prior works have

explored reconstruction-free inference (Bethi et al. 2021; Hu et al. 2021a; Zhang et al. 2022; Lu, Yuan, and Shi 2020; Okawara et al. 2020), most directly apply standard vision models to mosaic-like SCI data, leading to suboptimal results. For instance, in (Lu, Yuan, and Shi 2020), high-speed object motion in compressed highway footage led to recognition failures due to motion artifacts. Our proposed framework, CompDAE, on the other hand, leverages a Transformer-based encoder-decoder architecture to learn spatiotemporal features directly from noisy compressive measurements. The same encoder can be paired with different lightweight decoders for edge detection, depth estimation, or semantic segmentation—achieving both hardware and computational efficiency. In training the Transformer, we incorporate a rate-constrained training strategy inspired by the recent BackSlash algorithm (Wu, Wen, and Han 2025), leading to edge-deployment-friendly models that are model compression and pruning friendly, enabling low-complexity, high-efficiency vision tasks such as edge detection and depth estimation that are robust to a wide range of lighting and SNR conditions. Extensive evaluations across multiple datasets and tasks demonstrate that CompDAE consistently outperforms conventional APS and SCI-based pipelines, particularly under ultra-low-light conditions where existing methods fail.

## Related work

**Video Snapshot Compressed Imaging (SCI)** is a computational imaging technique that captures full frame rate video in a single 2D measurement by modulating each frame with a distinct mask and summing them. Reconstruction algorithms are then used to recover the original frames based on compressive sensing. Various CMOS-compatible designs have been proposed to enable on-chip SCI. For example, Dadkhah et al. (Dadkhah, Jamal Deen, and Shirani 2014) introduced a block-based CS method using a three-transistor APS and  $8 \times 8$  pseudo-random exposure, achieving a compact, low-power implementation but with limited flexibility and high reconstruction complexity under low-photon conditions. Yoshida et al. (Yoshida et al. 2020) developed quasi pixel-wise exposure control within  $8 \times 8$  blocks, though its fixed structure hampers noise cancellation in photon-limited settings. Zhang et al. (Zhang et al. 2016) implemented pixel-wise coded exposure entirely in CMOS with in-pixel memory, enabling ultra-low power operation but limiting adaptability due to a fixed single-on pattern. More recently, Liu et al. (Liu et al. 2024) proposed an adaptive optical architecture with dynamic mask selection, improving performance across lighting conditions at the cost of increased system size and photon loss. In contrast, our approach adopts a fixed-mask optical design and introduces a compressive denoising autoencoder built on spatiotemporal Transformers, enabling robust, high-quality video understanding directly from noisy compressive measurements, even under severe photon-limited conditions.

Recent advances in SCI have extended encoding strategies beyond simple binary masks. Multi-bit and multi-state schemes—such as Gray codes and progressive masks—offer greater dynamic range to support both low-light and normal-

light conditions. Wang et al. (Wang, Wang, and Yuan 2023) showed that deep learning can adapt encoding parameters in real time to varying illumination using high-refresh-rate digital mirror devices (DMDs). In parallel, more accurate noise modeling has emerged, with additive Gaussian (Inagaki et al. 2018) and Poisson (Liu et al. 2024) models better capturing low-light sensor behavior. End-to-end optimization of learnable masks has also been explored (Huang et al. 2022; Yoshida et al. 2018; Iliadis, Spinoulas, and Katsaggelos 2020). In contrast, our method uses fixed  $8 \times 8$  repeated binary masks on a DMD, simplifying hardware implementation while providing reliable, consistent modulation.

In video analysis, reconstruction-based methods first recover full video frames from compressive measurements before applying conventional frame-by-frame algorithms. For instance, Hu et al. (Hu et al. 2021b) perform object detection on reconstructed video, Lu et al. (Lu, Yuan, and Shi 2020) process restored footage for sequential tasks, and Kwan et al. (Kwan et al. 2019) use reconstructed images for target tracking. In contrast, reconstruction-free methods operate directly on compressive measurements: Liang et al. (Liang et al. 2022) and Zhang (Zhang et al. 2022) extract semantic features without full reconstruction, while Bethi et al. (Bethi et al. 2021) and Lu et al. (Lu, Yuan, and Shi 2020) conduct recognition tasks directly on compressed inputs. Our approach follows this latter direction, but goes further by extracting spatiotemporal semantic representations end-to-end, eliminating the need for explicit reconstruction entirely.

Reconstructing video from SCI measurements is an ill-posed inverse problem. Traditional model-based methods rely on iterative optimization (Liao, Li, and Carin 2014; Boyd et al. 2011) with handcrafted priors such as total variation (Yuan 2016) or non-local low-rank structures (Liu et al. 2018), but often suffer from poor quality and high computational cost. These limitations have led to deep learning-based approaches: GAP-net (Meng et al. 2020), DUN-3DUNet (Wu, Zhangt, and Mou 2021), and Two-stage (Zheng, Yang, and Yuan 2022) leverage deep unfolding for better speed and accuracy. STFormer (Wang et al. 2022) introduces space-time factorization and local self-attention to model spatiotemporal correlations efficiently. While Transformers (Vaswani et al. 2017) capture long-range dependencies, their high complexity poses challenges for large-scale color video. EfficientSCI (Wang, Cao, and Yuan 2023) addresses this by combining CNNs and Transformers with hierarchical residuals, achieving strong performance on UHD color video reconstruction.

**Denosing Autoencoders (DAEs)** learn robust representations by reconstructing clean inputs from corrupted versions (Vincent et al. 2008). Given a noisy input  $x_{noisy}$ , the encoder maps it to a latent code  $z = f(x_{noisy})$  which the decoder then uses to recover the original signal  $x_{clean}$ . DAEs are widely used in vision tasks for extracting noise-invariant features (Pathak et al. 2016; Chen et al. 2020; Dosovitskiy et al. 2020; He et al. 2022). Recent works apply Transformers (Vaswani et al. 2017) to unify vision and language modeling. iGPT (Chen et al. 2020) treats pixels as tokens, while ViT (Dosovitskiy et al. 2020) uses patches, enabling masked prediction. MAE (He et al. 2022) builds on DAE

principles with a masked autoencoding framework that reconstructs missing image patches from sparse visible inputs using an asymmetric encoder-decoder design, capturing high-level semantics efficiently.

**Rate-Constrained Training**, inspired by BackSlash (Wu, Wen, and Han 2025), introduces a regularization term based on Exp-Golomb coding to balance model accuracy and parameter compressibility. We adopt this strategy during training to guide the network toward compact, efficient representations, supporting both reconstruction and downstream vision tasks in our compressive sensing framework.

## Single Measurement SCI-based Computer Vision in Low-Lighting Conditions

### Imaging Pipeline and Noise

For gray-scale video SCI, we use coded aperture compressive temporal imaging (CACTI) (Llull et al. 2013) as an example. The frames of a video sequence are modulated temporally and spatially and then compressed to a single measurement. The number of coded frames for a single measurement is determined by the mask or different patterns on the DMD within the integration (exposure) time. Specifically, consider that  $T$  video frames are modulated by  $T$  different modulation patterns. Let  $\{\mathbf{X}_t\}_{t=1}^T \in \mathbb{R}^{n_x \times n_y}$  denote a  $T$ -frame high-speed scene to be captured in a single exposure time, where  $n_x, n_y$  represent the spatial resolution of each frame and  $T$  is the compression ratio (Cr) of the video SCI system. Then, the modulation process can be modeled as multiplying  $\{\mathbf{X}_t\}_{t=1}^T$  by pre-defined masks  $\{\mathbf{M}_t\}_{t=1}^T \in \mathbb{R}^{n_x \times n_y}$ ,

$$\mathbf{Y}_t = \mathbf{X}_t \odot \mathbf{M}_t, \quad (1)$$

where  $\{\mathbf{Y}_t\}_{t=1}^T \in \mathbb{R}^{n_x \times n_y}$  and  $\odot$  denote the modulated frames and element-wise Hadamard product, respectively. Modulated frames are then summed to a single measurement  $\mathbf{Y} \in \mathbb{R}^{n_x \times n_y}$ . Thus, the forward model of the video SCI system can be formulated as,

$$\mathbf{Y} = \sum_{t=1}^T \mathbf{X}_t \odot \mathbf{M}_t + \mathbf{N}, \quad (2)$$

where  $\mathbf{N} \in \mathbb{R}^{n_x \times n_y}$  denotes the measurement noise. In the context of photon-limited applications (such as low-light imaging), the Poisson-Gaussian model is generally used for raw-data digital imaging sensor data (Foi et al. 2008). In general, the noise term is composed of two mutually independent parts, a Poisson signal-dependent component  $\eta_p$  and a Gaussian signal-independent component  $\eta_g$ .

$$\mathbf{Y}_{\text{noisy}} = \sum_{t=1}^T (\mathbf{X}_t \odot \mathbf{M}_t + \eta_{p,t}) + \eta_g. \quad (3)$$

The distributions of these two components are characterized as follows,  $\alpha(\mathbf{X}_t \odot \mathbf{M}_t + \eta_{p,t}) \sim \mathcal{P}(\alpha(\mathbf{X}_t \odot \mathbf{M}_t))$ ,  $\eta_g \sim \mathcal{N}(0, \sigma)$ , where  $\alpha > 0$  and  $\sigma > 0$  are real scalar parameters and  $\mathcal{P}$  and  $\mathcal{N}$  Denote the Poisson and normal distributions.

## CompDAE: Visual Intelligence from Raw Temporal Measurements

At the core of our proposed SCI-based compressive computer vision system is CompDAE, a DAE (Vincent et al. 2008) that reconstructs the original clean spacetime data from its raw temporal compressive measurement captured by SCI sensors. Like all DAEs, our approach consists of an encoder that maps noisy raw measurements into a latent representation, and a decoder that reconstructs the original spacetime signal from this latent representation. Similar to the Masked Autoencoder (MAE) (He et al. 2022), we adopt an asymmetric design where the encoder operates both the measurement and modulation masks of the SCI system, while a lightweight decoder (with  $N < M/2$ ) reconstructs the full signal from the latent representation.

**Hardware-friendly mask design** Due to physical constraints, the masks or DMD responses to light are always nonnegative and bounded (Llull et al. 2013; Jiang, Raskutti, and Willett 2015). Moreover, practical SCI systems often employ binary-valued masks. Theoretical analysis shows that i.i.d. binary (Bernoulli) masks are feasible for signal recovery (Zhao and Jalali 2023), while the probability of non-zero entries  $\rho$  is related to reconstruction distortion and a hyperparameter in mask design. As illustrated in Figure 1, binary masks for the entire frame in CompDAE are generated by spatially replicating smaller binary sub-masks  $\{\mathbf{A}_t\}_{t=1}^T \in \{0, 1\}^{m_x \times m_y}$  in both directions, i.e.  $\mathbf{M}_t = \mathbf{J}_{n_x/m_x} \otimes \mathbf{A}_t$ , where  $\mathbf{J}_{n_x/m_x}$  is an all-ones matrix of size  $n_x/m_x$  and  $\otimes$  represents the Kronecker product.

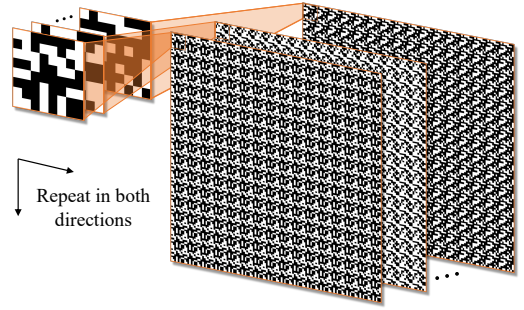


Figure 1: Construction of binary mask pattern.

**CompDAE encoder and decoder** Following STFormer, we adopt an estimation module to pre-process the measurement and masks, as in (Cheng et al. 2021, 2020). Our encoder consists of a token generation (TG) block using 3D CNNs, followed by stacked STFormer blocks that model spatial-temporal dependencies. Unlike STFormer, the estimation module comprises a Noise Level Mapping (NLM) for unified noise-adaptive training, and the decoder is used only during pre-training (Cheng et al. 2021) for reconstruction. To support diverse downstream tasks efficiently, we design the decoder with a few STFormer blocks followed by a convolutional layer. We adopt a partial fine-tuning strategy (He et al. 2022), updating only the decoder while keeping the encoder fixed. This asymmetric design enables task-specific decoders to be lightweight and fast to train, while still bene-

fitting from shared, robust spatiotemporal representations.

**Unified Noise-Adaptive Training Strategy** To support generalization and real-world deployment, we propose a unified training strategy that enables a single CompDAE model to handle diverse noise levels. The model takes a multi-channel input tensor comprising a signal estimate, a Gaussian noise map, and a Poisson noise proxy via Average Photon Count (APC). This design allows the network to learn noise-aware features and adapt dynamically to varying lighting and SNR conditions.

**Training-Time Compression (BackSlash)** We apply rate-constrained training (RCT), inspired by BackSlash (Wu, Wen, and Han 2025), to balance performance and model size. Using exponential-Golomb (EG) codes (Wen and Villasenor 1999), we regularize parameter sparsity by minimizing  $J(\theta) = L_{\text{task}}(\theta) + \lambda R(\theta)$ , where  $L_{\text{task}}(\theta)$  denotes the task-specific loss and the rate term is defined as  $R(\theta) = \frac{1}{N} \sum_{i=1}^N (|\theta_i| + \epsilon)^\nu$ , with  $N$  being the total number of parameters,  $\epsilon$  a small constant, and  $\nu$  the GG shape parameter. This explicit rate regularization encourages the compressibility of GG-distributed parameters. CompDAE learns directly from noisy, raw SCI measurements under varying SNRs. It generates tokenized video representations during pre-training, then fine-tunes lightweight decoders for pixel-level reconstruction, classification, or regression, supporting modular vision tasks under low-light conditions.

## Experiment Results

We evaluate CompDAE through self-supervised pre-training on the DAVIS2017 dataset (Pont-Tuset et al. 2017), using 90 videos (6242 frames at 480×894 resolution). We then apply transfer learning for two vision tasks: (i) edge detection and (ii) monocular depth estimation. For edge detection, high-quality ground truth maps are generated using DexiNed (Poma, Riba, and Sappa 2020), and the fine-tuned model is tested on six gray-scale benchmark datasets (Yuan et al. 2020). For depth estimation, we use RGB-guided depth completion on KITTI (Uhrig et al. 2017) to train and evaluate the model on simulated raw SCI measurements. We further test segmentation on Cityscapes (Cordts et al. 2016), where dense annotations exist only for sparse frames. Leveraging CompDAE’s temporal modeling, we fine-tune the segmentation decoder using limited training annotations, demonstrating strong generalization across time.

## Implementation Details

We train our model using PyTorch on a single NVIDIA A100 (80GB) GPU. Photon-limited measurements are generated following the process in Sec. , with Gaussian noise ( $\sigma = 0.01$ ) added by default to simulate sensor noise. Data augmentation includes random cropping, flipping, and APC variation. Training uses the Adam optimizer (Kinga, Adam et al. 2015) with an initial learning rate of 0.0001. For compressive sampling, we use 8-frame sequences at 128×128 resolution ( $\text{Cr} = 8$ ), sampled from the original sequence using a stride of 1 or 2 to preserve temporal redundancy.

Training consists of two stages: self-supervised pre-training on noisy measurements (80 epochs) and task-

specific fine-tuning. For edge detection, we fine-tune on 128×128 inputs for 40 epochs. For depth estimation, the KITTI data is resized to 256×256 and fine-tuned for 50 epochs. For semantic segmentation, we fix the encoder and train a PPM head (Zhao et al. 2017) on color Bayer measurements from Cityscapes (256×512) for 40 epochs.

We evaluate CompDAE using task-specific metrics. For edge detection, we report Optimal Dataset Scale (ODS) and Optimal Image Scale (OIS) F1-scores. Depth estimation performance is measured by AbsRel, RMSE, log10 error, and accuracy thresholds ( $\delta_1, \delta_2, \delta_3$ ). For segmentation, we use mean Intersection over Union (mIoU) and mean Pixel Accuracy (mPA).

## Comparison with conventional systems

We highlight the failure of conventional edge detection algorithms under ultra-low-light conditions. As shown in Figure 2, DexiNed struggles at low APC, producing noisy, indistinct edges, while CompDAE maintains clear structure. We further compare CompDAE with classical edge detectors (Canny (Canny 1986), RCF (Liu et al. 2017), BDCN (He et al. 2019)) and depth estimation methods (MiDaS (Birkel, Wofk, and Müller 2023), Unidepth (Piccinelli et al. 2024), Metric3D (Hu et al. 2024), LightedDepth (Zhu and Liu 2023)). Quantitative comparisons are given in Table 1, which shows that CompDAE outperforms conventional APS-based methods (Canny, RCF, BDCN, DexiNed) in ODS and OIS scores at APC = 20. Unlike frame-by-frame ISP-based approaches, CompDAE processes a single low-SNR measurement, yet still achieves superior edge detection under severe low-light conditions.

CompDAE effectively maintains high performance under low-light conditions.

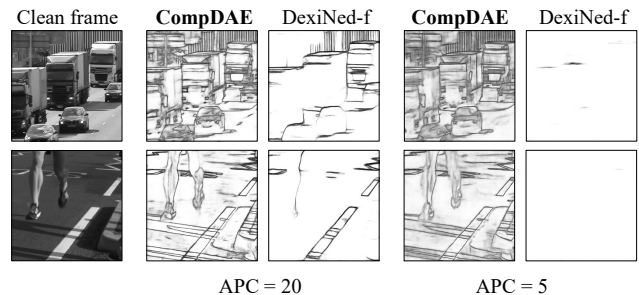


Figure 2: Comparison of edge detection results under different ultra-low-lighting conditions.

Method	ODS	OIS	Params (M)
Canny	0.450	0.455	-
BDCN	0.389	0.441	16.30
RCF	0.427	0.454	14.80
DexiNed	0.474	0.479	35.22
CompDAE	<b>0.690</b>	<b>0.704</b>	23.82

Table 1: Evaluation on gray-scale video benchmark datasets with our fine-tuned CompDAE.

Method	AbsRel	RMSE	log10	$\delta_1$	$\delta_2$	$\delta_3$
Unidepth	0.331	7.483	0.353	0.561	0.829	0.919
MiDaS	0.431	8.116	1.658	0.352	0.642	0.812
Metric3D	0.329	8.600	0.351	0.582	0.843	0.922
LightedDepth	0.361	12.016	0.743	0.521	0.635	0.731
CompDAE $_{N=0}$	0.309	7.203	0.368	0.670	0.812	0.894
CompDAE $_{N=1}$	<b>0.181</b>	<b>5.177</b>	<b>0.262</b>	<b>0.770</b>	<b>0.893</b>	<b>0.951</b>

Table 2: Evaluation on KITTI with fine-tuned CompDAE.

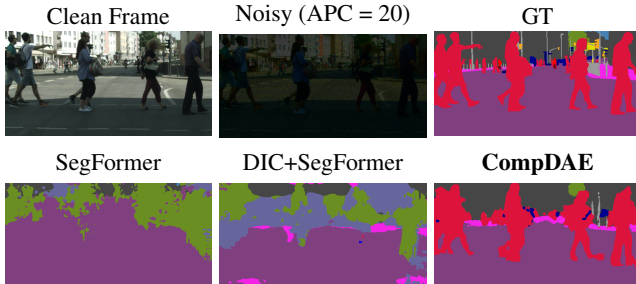


Figure 3: Qualitative comparison for semantic segmentation on Cityscapes.

Table 2 further shows that CompDAE with a decoder depth of  $N = 1$ , outperforms Unidepth and Metric3D in depth estimation under the same low-light setting, demonstrating its strong generalization across vision tasks. Notably, while Unidepth performs well at  $APC = 20$ , it requires 353.83M parameters, 15 times that of our model. Despite this, CompDAE ( $N = 0$ ) achieves comparable accuracy with far lower computational cost. Moreover, CompDAE boasts an inference time of 2.60 ms per frame, vastly outperforming Unidepth’s 63.90 ms, making CompDAE far more suitable for real-time applications.

To assess the encoder’s ability to capture semantic and temporal features beyond edges, we perform semantic segmentation using raw Bayer measurements. Given limited annotated video data, we extract features from a single annotated frame and fine-tune only the decoder. As shown in Figure 3, our method produces more accurate and plausible segmentation maps than the baseline. At  $APC = 20$ , CompDAE achieves 30.43% mIoU and 82.49% mPA, significantly outperforming SegFormer (6.65% mIoU, 58.09% mPA), demonstrating strong semantic understanding under compressive sensing constraints.

### Ablation study observations

We conduct controlled ablation studies by modifying key components of CompDAE, using shorter training schedules for broader experimentation. Unless noted, both NLM and BackSlash are excluded. The results reveal several notable insights.

As mentioned earlier, decoder depth  $N$  refers to the number of STFormer blocks in the decoder. Within our system framework, we use partial fine-tuning (Zhang, Isola, and Efros 2016; He et al. 2022) to optimize efficiency. Our asymmetric setup (*i.e.*,  $N < M/2$  with  $M = 4$ ) keeps the decoder lightweight and adaptable. As shown in Table 3a, increas-

ing  $N$  initially improves ODS and OIS scores, peaking at depth 2. Further increasing depth to 3 slightly degrades performance, suggesting diminishing returns relative to added complexity.

Table 3b shows the impact of compression ratio (Cr). A higher Cr reduces data bandwidth but increases compression. We find that  $Cr = 8$  offers the best trade-off, preserving scene dynamics while minimizing information loss, particularly under low-light, low-SNR conditions where traditional methods struggle. Consistent Cr values during training and testing yield optimal performance, while mismatches significantly degrade results. These findings highlight the importance of aligning Cr settings to maintain accuracy and preserve the system’s low-complexity, high-speed benefits.

Table 3c examines the impact of mask density, defined by  $\rho$ , the probability of non-zero entries in the  $8 \times 8$  binary masks. While higher  $\rho$  allows more light and potentially increases photon counts, it may reduce spatial modulation. Our results show that within the 0.3-0.5 range,  $\rho$  has minimal effect on reconstruction quality, even under low-light conditions. This supports findings in (Iliadis, Spinoulas, and Katsaggelos 2020) that smoother sensing patterns can maintain performance regardless of  $\rho$ , highlighting the robustness of our system across different mask densities.

### Training Strategy Comparisons

We assess the effect of the BackSlash rate-constrained training strategy on performance. Two model types were tested: APC-specific models trained at fixed APC levels (5, 10, 20) and a unified model trained across a wide APC range (1-60) and evaluated at the same levels. Compression efficiency is measured by Effective Golomb Compression Rate (EGCR), where a lower average Exp-Golomb code length indicates higher compactness. Without BackSlash, both model types already perform well, with the unified model showing strong generalization. However, applying BackSlash throughout training slightly degrades edge detection. To address this, we adopt a Half BackSlash strategy—applied only during the early training phase—which preserves accuracy while improving parameter efficiency. As shown in Table 4, this approach balances compactness and task performance under varied lighting conditions.

### Comparison with Other SCI-based Methods

To highlight the advantages of CompDAE, we compare it against representative methods in two aspects: (1) its superior performance as an end-to-end alternative to traditional two-stage SCI approaches, and (2) its robustness as a multi-task, multi-condition platform. All experiments use our unified model trained with the Half BackSlash strategy for consistent evaluation.

**End-to-End Paradigm vs. Two-Stage Pipeline** A common SCI vision approach uses a two-stage pipeline: reconstruct the video, then apply a vision model. We compare our end-to-end CompDAE to this baseline, using DIC (Liu et al. 2024) for low-light reconstruction followed by standard task-specific models.

Depth	ODS	OIS
$N = 0$	0.672	0.685
$N = 1$	0.681	0.694
$N = 2$	0.695	0.709
$N = 3$	0.686	0.698

(a) Impact of Decoder Depth.

Cr	4		8		16	
	ODS	OIS	ODS	OIS	ODS	OIS
4	0.669	0.682	0.587	0.593	0.459	0.497
8	-	-	0.672	0.685	0.513	0.538
16	-	-	-	-	0.612	0.617

(b) Impact of Compression Ratio (Cr).

$\rho$	ODS	OIS
0.3	0.673	0.680
0.4	0.638	0.652
0.5	0.672	0.685

(c) Impact of Mask Pattern Density.

Table 3: Ablation studies on key hyperparameters

Model Type	Strategy	APC = 5			APC = 10			APC = 20		
		ODS	OIS	EGCR(%)	ODS	OIS	EGCR(%)	ODS	OIS	EGCR(%)
APC-specific	w/o BackSlash	0.660	0.677	-	0.676	0.691	-	0.696	0.712	-
	w/ BackSlash	0.629	0.642	83.91	0.653	0.672	83.93	0.674	0.691	83.93
	half BackSlash	0.646	0.661	48.66	0.666	0.684	48.31	0.690	0.704	48.70
Unified	w/o BackSlash	0.638	0.656	-	0.669	0.687	-	0.683	0.701	-
	w/ BackSlash	0.606	0.621	83.63	0.634	0.651	83.63	0.659	.674	83.63
	half BackSlash	0.621	0.639	50.06	0.650	0.669	50.06	0.670	0.685	50.06

Table 4: Edge Detection Performance comparison for different training strategies under varying APC test conditions.

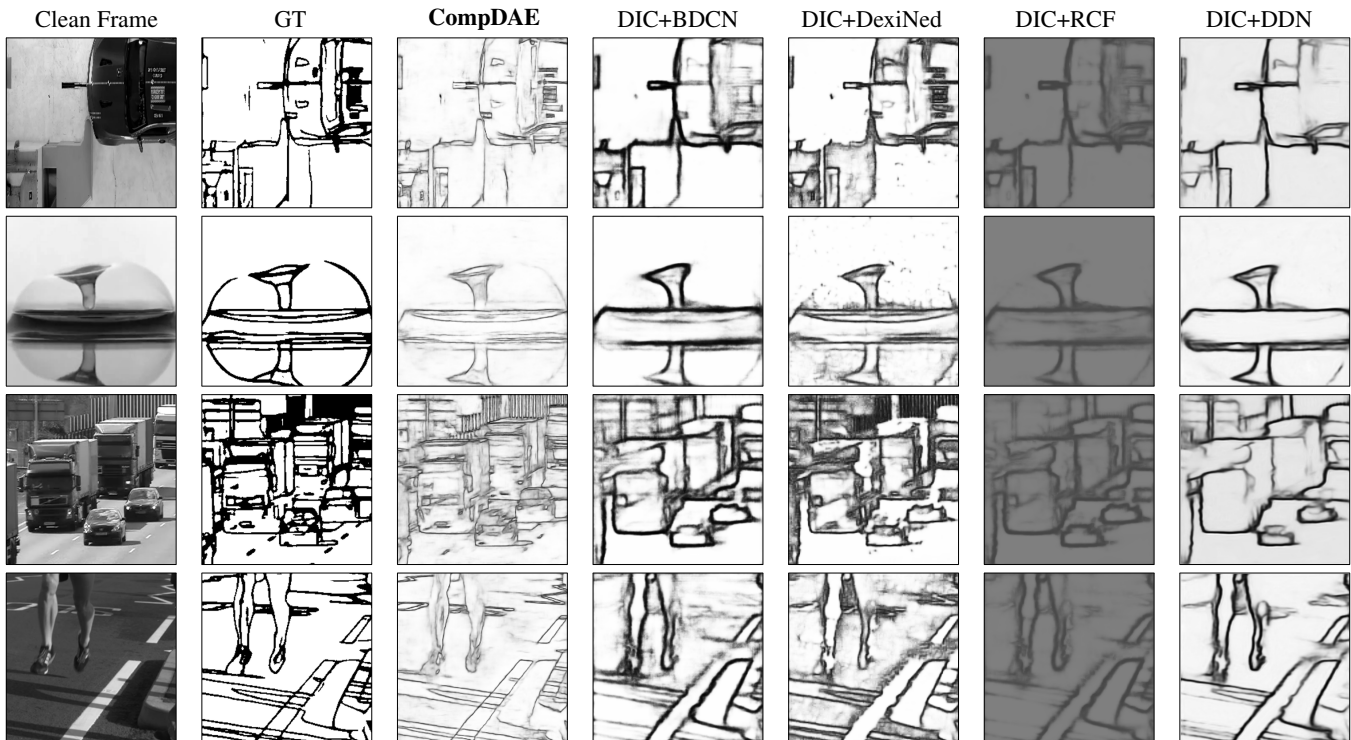


Figure 4: Qualitative comparison of edge detection results on several benchmark datasets.

Tables 5a and 5b show that CompDAE consistently outperforms two-stage baselines across edge detection and depth estimation. For semantic segmentation, it achieves 30.43% mIoU and 82.49% mPA, far surpassing the DIC+SegFormer baseline (6.60% mIoU, 45.37% mPA). Visual comparisons further confirm these gains: CompDAE produces cleaner edges and more accurate depth maps than DIC-based pipelines. These results highlight the effectiveness of our end-to-end design. By extracting task-specific features directly from compressive measurements, Comp-

DAE avoids reconstruction artifacts, improving both accuracy and efficiency while preserving privacy.

**Versatility and Robustness of CompDAE** Beyond outperforming two-stage pipelines, CompDAE proves to be a versatile and robust general-purpose framework. CompDAE pairs a shared measurement encoder with lightweight, task-specific decoders to handle edge detection, depth estimation, and semantic segmentation, demonstrating the generality of its learned representations from raw compressive data. Fur-

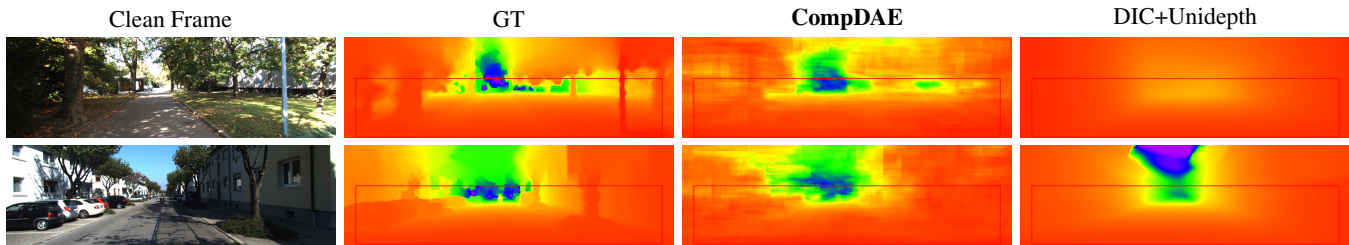


Figure 5: Qualitative comparison of depth estimation results on KITTI test dataset.

Method	APC = 5		APC = 10		APC = 20	
	ODS	OIS	ODS	OIS	ODS	OIS
DIC+BDCN	0.489	0.508	0.501	0.521	0.509	0.528
DIC+DexiNed	0.460	0.473	0.507	0.517	0.547	0.554
DIC+RCF	0.471	0.497	0.492	0.521	0.498	0.528
DIC+DDN	0.433	0.484	0.459	0.496	0.487	0.509
CompDAE	<b>0.621</b>	<b>0.639</b>	<b>0.650</b>	<b>0.669</b>	<b>0.670</b>	<b>0.685</b>

(a) Edge Detection Performance Comparison.

Method	AbsRel	RMSE	log10	$\delta_1$	$\delta_2$	$\delta_3$
DIC+Unidepth	0.183	6.514	0.453	0.741	0.842	0.875
DIC+MiDaS	0.415	7.961	1.699	0.337	0.649	0.827
DIC+Metric3D	0.354	8.693	0.359	0.560	0.803	0.892
DIC+LightedDepth	0.867	15.742	0.818	0.513	0.602	0.673
CompDAE	<b>0.181</b>	<b>5.177</b>	<b>0.262</b>	<b>0.770</b>	<b>0.893</b>	<b>0.951</b>

(b) Depth Estimation Performance Comparison.

Table 5: Quantitative comparison for downstream tasks.

thermore, as shown in Table 5a, the unified model maintains strong performance across varying low-light conditions (APC = 5, 10, 20), thanks to our unified training strategy that adapts to diverse noise levels. In summary, CompDAE offers an efficient, end-to-end solution for direct-from-sensor vision across tasks and lighting conditions.

### Results on Real-World Photon-Limited Video Data

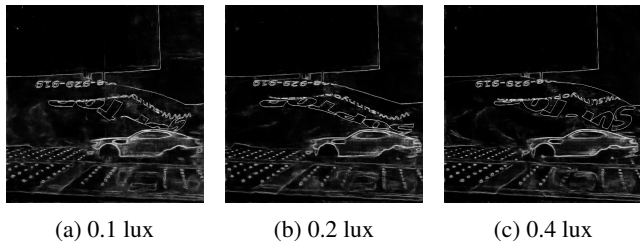


Figure 6: Results of edge detection on the real-world SPAD dataset under different extreme photon-starved conditions.

To assess real-world performance under extreme low-light, we tested CompDAE on video captured by the SPAD512S camera, which provides photon-level imaging at 512×512 resolution and 200 fps. SPAD data is inherently noisy, posing challenges for conventional methods. As shown in Figure 6, CompDAE delivers robust results across varied low-light scenes, demonstrating its practical effectiveness and ability to generalize from simulation to real-world photon-limited data.

### Discussions

This paper addresses key limitations of traditional SCI systems, which, though high-speed and low-power, struggle under low-light, low-SNR conditions and face hardware chal-

lenges due to large frame-sized masks. To address this, we propose a practical design using fixed 8×8 masks, avoiding external memory access and enabling efficient hardware implementation. We introduce CompDAE, a hybrid Transformer-CNN system built on STFormer, which directly processes raw compressive measurements to perform vision tasks like edge detection and depth estimation without full reconstruction. By explicitly modeling noise and leveraging compressed data, CompDAE delivers strong performance in challenging low-light scenarios where conventional methods fail. Across tasks and datasets, CompDAE matches or exceeds traditional approaches—especially under extreme photon limitations—while significantly reducing model size and complexity. Its modular design supports a universal encoder for sensing and task-specific decoders for diverse vision applications, offering a flexible and scalable framework for future SCI-based vision systems.

Our proposed CompDAE effectively reconstructs multi-frame sequences directly from compressive measurements under low-SNR, photon-limited conditions. By operating in the measurement domain, it avoids full RGB reconstruction, significantly reducing bandwidth and computation—ideal for real-time applications like surveillance, autonomous driving, and mobile devices. Combining CNNs with spatiotemporal Transformers, CompDAE achieves robust denoising and representation in extreme low-light scenarios. Its privacy-preserving nature—by never producing high-fidelity RGB frames—makes it especially suited for sensitive applications where visual confidentiality is critical.

Despite these strengths, CompDAE uses fixed-sized binary masks, which, while hardware-friendly, limit adaptability across tasks and scenes. Future work may explore adaptive, learnable masks co-optimized with the networks, along with real-time dynamic sensing hardware, enabling more intelligent and flexible compressive vision systems.

## References

- Baraniuk, R.; Davenport, M.; DeVore, R.; and Wakin, M. 2008. A Simple Proof of the Restricted Isometry Property for Random Matrices. *Constructive Approximation*, 28(3): 253–263.
- Bethi, Y. R. T.; Narayanan, S.; Rangan, V.; Chakraborty, A.; and Thakur, C. S. 2021. Real-time object detection and localization in compressive sensed video. In *ICIP*, 1489–1493. IEEE.
- Birkel, R.; Wofk, D.; and Müller, M. 2023. Midas v3. 1—a model zoo for robust monocular relative depth estimation. *arXiv preprint arXiv:2307.14460*.
- Bochkovskii, A.; Delaunoy, A.; Germain, H.; Santos, M.; Zhou, Y.; Richter, S. R.; and Koltun, V. 2024. Depth Pro: Sharp Monocular Metric Depth in Less Than a Second. *arXiv preprint arXiv:2410.02073*.
- Boyd, S.; Parikh, N.; Chu, E.; Peleato, B.; Eckstein, J.; et al. 2011. Distributed optimization and statistical learning via the alternating direction method of multipliers. *Foundations and Trends in Machine Learning*, 3(1): 1–122.
- Candes, E.; and Tao, T. 2005. Decoding by linear programming. *IEEE Transactions on Information Theory*, 51(12): 4203–4215.
- Candès, E. J.; Romberg, J. K.; and Tao, T. 2006. Stable signal recovery from incomplete and inaccurate measurements. *Communications on Pure and Applied Mathematics*, 59(8): 1207–1223.
- Canny, J. 1986. A computational approach to edge detection. *IEEE TPAMI*, PAMI-8(6): 679–698.
- Chen, M.; Radford, A.; Child, R.; Wu, J.; Jun, H.; Luan, D.; and Sutskever, I. 2020. Generative pretraining from pixels. In *ICML*, 1691–1703. PMLR.
- Cheng, Z.; Chen, B.; Liu, G.; Zhang, H.; Lu, R.; Wang, Z.; and Yuan, X. 2021. Memory-efficient network for large-scale video compressive sensing. In *CVPR*, 16246–16255.
- Cheng, Z.; Lu, R.; Wang, Z.; Zhang, H.; Chen, B.; Meng, Z.; and Yuan, X. 2020. BIRNAT: Bidirectional recurrent neural networks with adversarial training for video snapshot compressive imaging. In *ECCV*, 258–275. Springer.
- Cordts, M.; Omran, M.; Ramos, S.; Rehfeld, T.; Enzweiler, M.; Benenson, R.; Franke, U.; Roth, S.; and Schiele, B. 2016. The Cityscapes Dataset for Semantic Urban Scene Understanding. In *CVPR*.
- Dadkhah, M.; Jamal Deen, M.; and Shirani, S. 2014. Block-Based CS in a CMOS Image Sensor. *IEEE Sensors Journal*, 14(8): 2897–2909.
- Dong, X.; Wang, G.; Pang, Y.; Li, W.; Wen, J.; Meng, W.; and Lu, Y. 2011. Fast efficient algorithm for enhancement of low lighting video. In *ICME*. IEEE.
- Dosovitskiy, A.; Beyer, L.; Kolesnikov, A.; Weissenborn, D.; Zhai, X.; Unterthiner, T.; Dehghani, M.; Minderer, M.; Heigold, G.; Gelly, S.; Uszkoreit, J.; and Hounsby, N. 2020. An Image is Worth 16x16 Words: Transformers for Image Recognition at Scale. *arXiv preprint arXiv:2010.11929*.
- Foi, A.; Trimeche, M.; Katkovnik, V.; and Egiazarian, K. 2008. Practical Poissonian-Gaussian noise modeling and fitting for single-image raw-data. *IEEE TIP*, 17(10): 1737–1754.
- Gao, L.; Liang, J.; Li, C.; and Wang, L. V. 2014. Single-shot compressed ultrafast photography at one hundred billion frames per second. *Nature*, 516(7529): 74–77.
- Girshick, R.; Donahue, J.; Darrell, T.; and Malik, J. 2014. Rich feature hierarchies for accurate object detection and semantic segmentation. In *CVPR*, 580–587.
- Gulve, R.; Sarhangnejad, N.; Dutta, G.; Sakr, M.; Nguyen, D.; Rangel, R.; Chen, W.; Xia, Z.; Wei, M.; Gusev, N.; Lin, E. Y. H.; Sun, X.; Hanxu, L.; Katic, N.; Abdelhadi, A.; Moshovos, A.; Kutulakos, K. N.; and Genov, R. 2022. A 39,000 Subexposures/s CMOS Image Sensor with Dual-tap Coded-exposure Data-memory Pixel for Adaptive Single-shot Computational Imaging. In *2022 IEEE Symposium on VLSI Technology and Circuits (VLSI Technology and Circuits)*, 78–79.
- Guo, B.; Han, Y.; and Wen, J. 2019. Agem: Solving linear inverse problems via deep priors and sampling. *NeurIPS*, 32.
- He, J.; Zhang, S.; Yang, M.; Shan, Y.; and Huang, T. 2019. Bi-directional cascade network for perceptual edge detection. In *CVPR*, 3828–3837.
- He, K.; Chen, X.; Xie, S.; Li, Y.; Dollár, P.; and Girshick, R. 2022. Masked autoencoders are scalable vision learners. In *CVPR*, 16000–16009.
- Hitomi, Y.; Gu, J.; Gupta, M.; Mitsunaga, T.; and Nayar, S. K. 2011. Video from a single coded exposure photograph using a learned over-complete dictionary. In *ICCV*, 287–294.
- Hu, C.; Huang, H.; Chen, M.; Yang, S.; and Chen, H. 2021a. Video object detection from one single image through optoelectronic neural network. *APL Photonics*, 6(4).
- Hu, C.; Huang, H.; Chen, M.; Yang, S.; and Chen, H. 2021b. Video object detection from one single image through optoelectronic neural network. *APL Photonics*, 6(4): 046104.
- Hu, M.; Yin, W.; Zhang, C.; Cai, Z.; Long, X.; Chen, H.; Wang, K.; Yu, G.; Shen, C.; and Shen, S. 2024. Metric3d v2: A versatile monocular geometric foundation model for zero-shot metric depth and surface normal estimation. *IEEE Transactions on Pattern Analysis and Machine Intelligence*.
- Huang, H.; Hu, C.; Jingwei, L.; Dong, X.; and Chen, H. 2022. CoCoCs: co-optimized compressive imaging driven by high-level vision. *Optics Express*, 30: 30894–30910.
- Iliadis, M.; Spinoulas, L.; and Katsaggelos, A. K. 2020. Deepbinarymask: Learning a binary mask for video compressive sensing. *Digital Signal Processing*, 96: 102591.
- Inagaki, Y.; Kobayashi, Y.; Takahashi, K.; Fujii, T.; and Nagahara, H. 2018. Learning to Capture Light Fields Through a Coded Aperture Camera. In *ECCV*, 431–448. ISBN 978-3-030-01234-2.
- Jiang, X.; Raskutti, G.; and Willett, R. 2015. Minimax optimal rates for Poisson inverse problems with physical constraints. *IEEE TIP*, 61(8): 4458–4474.

- Karpathy, A.; Toderici, G.; Shetty, S.; Leung, T.; Sukthankar, R.; and Fei-Fei, L. 2014. Large-scale video classification with convolutional neural networks. In *CVPR*, 1725–1732.
- Khademi, W.; Rao, S.; Minnerath, C.; Hagen, G.; and Ventura, J. 2021. Self-supervised poisson-gaussian denoising. In *WACV*, 2131–2139.
- Kinga, D.; Adam, J. B.; et al. 2015. A method for stochastic optimization. In *ICLR*, volume 5, 6. San Diego, California.
- Kwan, C.; Chou, B.; Yang, J.; Rangamani, A.; Tran, T.; Zhang, J.; and Etienne-Cummings, R. 2019. Target tracking and classification using compressive measurements of MWIR and LWIR coded aperture cameras. *Journal of Signal and Information Processing*, 10(3): 73–95.
- Li, Y.; Guo, B.; Wen, J.; Xia, Z.; Liu, S.; and Han, Y. 2021. Learning model-blind temporal denoisers without ground truths. In *ICASSP*, 2055–2059. IEEE.
- Liang, Y.; Huang, H.; Jingwei, L.; Dong, X.; Chen, M.; Yang, S.; and Chen, H. 2022. Action recognition based on discrete cosine transform by optical pixel-wise encoding. *APL Photonics*, 7.
- Liao, X.; Li, H.; and Carin, L. 2014. Generalized alternating projection for weighted-2,1 minimization with applications to model-based compressive sensing. *SIAM Journal on Imaging Sciences*, 7(2): 797–823.
- Liu, X.; Zhu, M.; Zheng, S.; Luo, R.; Wu, H.; and Yuan, X. 2024. Video snapshot compressive imaging using adaptive progressive coding for high-quality reconstruction under different illumination circumstances. *Opt. Lett.*, 49(1): 85–88.
- Liu, Y.; Cheng, M.-M.; Hu, X.; Wang, K.; and Bai, X. 2017. Richer convolutional features for edge detection. In *Proceedings of the IEEE conference on computer vision and pattern recognition*, 3000–3009.
- Liu, Y.; Yuan, X.; Suo, J.; Brady, D. J.; and Dai, Q. 2018. Rank minimization for snapshot compressive imaging. *IEEE TPAMI*, 41(12): 2990–3006.
- Llull, P.; Liao, X.; Yuan, X.; Yang, J.; Kittle, D.; Carin, L.; Sapiro, G.; and Brady, D. J. 2013. Coded aperture compressive temporal imaging. *Optics express*, 21(9): 10526–10545.
- Lu, S.; Yuan, X.; and Shi, W. 2020. Edge compression: An integrated framework for compressive imaging processing on cavs. In *2020 IEEE/ACM Symposium on Edge Computing (SEC)*, 125–138. IEEE.
- Meng, Z.; Qiao, M.; Ma, J.; Yu, Z.; Xu, K.; and Yuan, X. 2020. Snapshot multispectral endomicroscopy. *Opt. Lett.*, 45(14): 3897–3900.
- Okawara, T.; Yoshida, M.; Nagahara, H.; and Yagi, Y. 2020. Action recognition from a single coded image. In *ICCP*, 1–11. IEEE.
- Ottewill, A.; and Rahman, M. 1997. Correlation Function and Power Spectrum of Non-Stationary Shot Noise. Technical Report LIGO-T970085-00-D, LIGO Project, California Institute of Technology and Massachusetts Institute of Technology. Preliminary version, printed June 12, 1997; internal technical note.
- Pathak, D.; Krahenbuhl, P.; Donahue, J.; Darrell, T.; and Efros, A. A. 2016. Context encoders: Feature learning by inpainting. In *CVPR*, 2536–2544.
- Piccinelli, L.; Yang, Y.-H.; Sakaridis, C.; Segu, M.; Li, S.; Gool, L. V.; and Yu, F. 2024. UniDepth: Universal Monocular Metric Depth Estimation. In *CVPR*, 10106–10116.
- Poma, X. S.; Riba, E.; and Sappa, A. 2020. Dense extreme inception network: Towards a robust cnn model for edge detection. In *WACV*, 1923–1932.
- Pont-Tuset, J.; Perazzi, F.; Caelles, S.; Arbeláez, P.; Sorkine-Hornung, A.; and Van Gool, L. 2017. The 2017 DAVIS Challenge on Video Object Segmentation. *arXiv preprint arXiv:1704.00675*.
- Reddy, D.; Veeraraghavan, A.; and Chellappa, R. 2011. P2C2: Programmable pixel compressive camera for high speed imaging. In *CVPR*, 329–336.
- Sun, L.; Wu, F.; Ding, W.; Li, X.; Lin, J.; Dong, W.; and Shi, G. 2024. Multi-Scale Spatio-Temporal Memory Network for Lightweight Video Denoising. *IEEE Transactions on Image Processing*, 33: 5810–5823.
- Uhrig, J.; Schneider, N.; Schneider, L.; Franke, U.; Brox, T.; and Geiger, A. 2017. Sparsity Invariant CNNs. In *International Conference on 3D Vision (3DV)*.
- Vaswani, A.; Shazeer, N.; Parmar, N.; Uszkoreit, J.; Jones, L.; Gomez, A. N.; Kaiser, L.; and Polosukhin, I. 2017. Attention is all you need. In *NeurIPS*, 6000–6010. Curran Associates Inc.
- Vincent, P.; Larochelle, H.; Bengio, Y.; and Manzagol, P.-A. 2008. Extracting and composing robust features with denoising autoencoders. In *ICML*, 1096–1103.
- Wang, L.; Cao, M.; and Yuan, X. 2023. Efficientsci: Densely connected network with space-time factorization for large-scale video snapshot compressive imaging. In *CVPR*, 18477–18486.
- Wang, L.; Cao, M.; Zhong, Y.; and Yuan, X. 2022. Spatial-temporal transformer for video snapshot compressive imaging. *IEEE TPAMI*, 45(7): 9072–9089.
- Wang, N.; and Yeung, D.-Y. 2013. Learning a deep compact image representation for visual tracking. *NeurIPS*, 26.
- Wang, P.; Wang, L.; and Yuan, X. 2023. Deep Optics for Video Snapshot Compressive Imaging. In *ICCV*, 10612–10622.
- Wen, J.; and Villasenor, J. 1999. Structured prefix codes for quantized low-shape-parameter generalized Gaussian sources. *IEEE Transactions on Information Theory*, 45(4): 1307–1314.
- Wu, J.; Wen, J.; and Han, Y. 2025. BackSlash: Rate Constrained Optimized Training of Large Language Models.
- Wu, Z.; Zhang, J.; and Mou, C. 2021. Dense deep unfolding network with 3D-CNN prior for snapshot compressive imaging. In *ICCV*. IEEE.
- Yoshida, M.; Sonoda, T.; Nagahara, H.; Endo, K.; Sugiyama, Y.; and Taniguchi, R.-i. 2020. High-Speed Imaging Using CMOS Image Sensor With Quasi Pixel-Wise Exposure. *IEEE Transactions on Computational Imaging*, 6: 463–476.

Yoshida, M.; Torii, A.; Okutomi, M.; Endo, K.; Sugiyama, Y.; Taniguchi, R.; and Nagahara, H. 2018. Joint optimization for compressive video sensing and reconstruction under hardware constraints. In Hebert, M.; Ferrari, V.; Sminchisescu, C.; and Weiss, Y., eds., *ECCV*, Lecture Notes in Computer Science (including subseries Lecture Notes in Artificial Intelligence and Lecture Notes in Bioinformatics), 649–663. Germany: Springer Verlag. ISBN 9783030012489. Publisher Copyright: © Springer Nature Switzerland AG 2018.; 15th European Conference on Computer Vision, ECCV 2018 ; Conference date: 08-09-2018 Through 14-09-2018.

Yuan, X. 2016. Generalized alternating projection based total variation minimization for compressive sensing. In *ICIP*, 2539–2543. IEEE.

Yuan, X.; Liu, Y.; Suo, J.; and Dai, Q. 2020. Plug-and-play algorithms for large-scale snapshot compressive imaging. In *CVPR*, 1447–1457.

Yuan, X.; and Pang, S. 2016. Structured illumination temporal compressive microscopy. *Biomed. Opt. Express*, 7(3): 746–758.

Zhang, J.; Xiong, T.; Tran, T.; Chin, S.; and Etienne-Cummings, R. 2016. Compact all-CMOS spatiotemporal compressive sensing video camera with pixel-wise coded exposure. *Optics Express*, 24: 9013–9024.

Zhang, R.; Isola, P.; and Efros, A. A. 2016. Colorful image colorization. In *ECCV*, 649–666. Springer.

Zhang, Z.; Zhang, B.; Yuan, X.; Zheng, S.; Su, X.; Suo, J.; Brady, D. J.; and Dai, Q. 2022. From compressive sampling to compressive tasking: retrieving semantics in compressed domain with low bandwidth. *Photonix*, 3(1): 19.

Zhao, H.; Shi, J.; Qi, X.; Wang, X.; and Jia, J. 2017. Pyramid Scene Parsing Network. In *CVPR*, 6230–6239.

Zhao, M.; and Jalali, S. 2023. Theoretical analysis of binary masks in snapshot compressive imaging systems. In *2023 59th Annual Allerton Conference on Communication, Control, and Computing (Allerton)*, 1–8. IEEE.

Zheng, S.; Yang, X.; and Yuan, X. 2022. Two-Stage is Enough: A Concise Deep Unfolding Reconstruction Network for Flexible Video Compressive Sensing. *arXiv preprint arXiv:2201.05810*.

Zhu, S.; and Liu, X. 2023. LightedDepth: Video Depth Estimation in light of Limited Inference View Angles. In *CVPR*.